THE JOURNAL OF PHYSICAL CHEMISTRY B

Article

pubs.acs.org/JPCB

# Accurate Quadrupolar NMR Relaxation Rates of Aqueous Cations from Classical Molecular Dynamics

Antoine Carof,[†,‡] Mathieu Salanne,[†,‡] Thibault Charpentier,[§] and Benjamin Rotenberg*[,†,‡]

[†]Sorbonne Universités, UPMC Univ. Paris 06, UMR 8234 PHENIX, 75005 Paris, France

[‡]CNRS, UMR 8234 PHENIX, 75005 Paris, France

[§]CEA, IRAMIS, NIMBE, LSDRM, UMR CEA-CNRS 3299, F-91191 Gif-sur-Yvette cedex, France

**ABSTRACT:** Nuclear magnetic resonance (NMR) relaxation rates encode information about the collective and local dynamics around nuclei. Provided a suitable microscopic model is available, this allows investigating, e.g., the solvation shell dynamics around aqueous ions. Previous attempts with molecular dynamics simulations faced the double challenge of calculating accurately the microscopic properties governing the relaxation process, such as the electric field gradient (EFG) at the nucleus, and of sampling the trajectories over sufficiently long times. Here we show how to compute the NMR relaxation rate from classical molecular dynamics simulations. We use a recently derived force field parametrized on ab initio calculations and show that the EFG predicted by this force field can be used to accurately estimate the one computed by DFT using the PAW method where the electronic structure is described explicitly. The predicted relaxation rates for aqueous alkaline and alkaline Earth cations are in good agreement with experimental data. Our approach opens the way to the quantitative interpretation of these rates with molecular simulation.

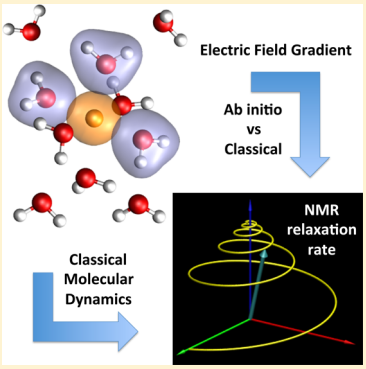


## 1. INTRODUCTION

Nuclear magnetic resonance (NMR) relaxation rates encode information on the microscopic dynamics around nuclei.[1] However, the interpretation of experimental measurements usually relies on simple models, e.g., Brownian rotational diffusion, which may not apply down to the molecular scale.[2] Hence, the amount of microscopic information that can be retrieved from such experiments remains rather limited in practice. For nuclei with spin $I \geq 1$, the main relaxation mechanism is the quadrupolar interaction involving the coupling of the nuclear quadrupole moment $eQ$ with the electric field gradient (EFG) $V_{\alpha\beta}$ at the nucleus. In the so-called extreme narrowing limit, the longitudinal and transverse magnetizations decay exponentially. The corresponding rates $1/T_1$ and $1/T_2$ reflect the fluctuations in time of the EFG and thus probe the environment of the nuclei. For an isotropic system, both rates are equal and usually written as[1,3]

$$\frac{1}{T_1} = \frac{3}{8}\frac{2I+3}{I^2(2I-1)}\left(\frac{eQ}{\hbar}\right)^2 \langle {V_{zz}}^2 \rangle \tau_c \qquad (1)$$

with $e$ being the elementary charge, $\hbar$ Planck's constant, $I$ the nuclear spin, $eQ$ the nuclear quadrupole moment of the nucleus under consideration, and $V_{zz}$ the $zz$ Cartesian component of the EFG in the laboratory frame and where the brackets denote an ensemble average. The correlation time $\tau_c$ of the EFG autocorrelation function (acf) is given by

$$\tau_c = \frac{\int_0^\infty \langle V_{zz}(0) V_{zz}(t) \rangle \, dt}{\langle {V_{zz}}^2 \rangle} \qquad (2)$$

From the modeling point of view, the challenge is then to model the EFG acf in order to extract relevant information from the experimental relaxation rates. Here we show how classical molecular dynamics (MD) simulation calibrated on ab initio data can provide this quantity efficiently, by combining an accurate evaluation of the EFG for each configuration, a realistic description of the microscopic dynamics, and a moderate computational cost allowing for the sampling of trajectories over the required time scales.

Due to their ubiquity in chemistry or biology, the case of quadrupolar aqueous ions ($^7Li^+$, $^{23}Na^+$, $^{25}Mg^{2+}$, $^{39}K^+$, $^{133}Cs^+$, ...) has attracted a lot of attention since the early days of NMR.[4−7] Various NMR techniques can be used to probe their environment in complex materials such as zeolites,[8,9] clays,[10−12] and glasses[13,14] or their binding to biological molecules such as DNA.[15] Classical molecular simulations have demonstrated the shortcomings of theories based on continuous descriptions of the medium, such as a dielectric continuum or a viscous implicit solvent,[16−18] or based on the dynamics of single water molecules,[4,5] even in the simplest case of dilute electrolyte solutions. The local, molecular structure of the solvent around the ion cannot be neglected.[19−21] Engström et al.[22] as well as Roberts and Schnitker[23] underlined the role of the symmetry of the hydration shell on the resulting EFG at the nucleus site and showed that cross-correlations between water molecules around the ion cannot be neglected so that the

**Received:** October 19, 2014
**Revised:** October 23, 2014
**Published:** October 23, 2014

   dx.doi.org/10.1021/jp5105054 | J. Phys. Chem. B 2014, 118, 13252−13257

collective dynamics of the shell should be taken into account. In addition, they found that the decay of the EFG acf displays two characteristic times, in contrast with the standard assumption of monoexponential decay (Debye model). Until now, no clear physical interpretation was proposed for this two-step decay, even if this behavior may be found for related properties (e.g., solvation energy, forces, etc.). In the case of $^{7}Li^{+}$, the relative contributions of dipole−dipole and quadrupolar relaxation mechanisms have also been examined using classical MD.[24,25]

For such simulations to quantitatively reproduce the experimental results, thereby allowing the extraction of microscopic information from the data, it is essential that the model captures both the EFG on the nucleus for any given configuration and the microscopic dynamics of the system. In addition, the associated computational cost should not impede the proper sampling of trajectories required to compute the EFG acf. Since the fastest characteristic time of the EFG acf (typically tens of fs, see below) is larger than the MD time step (typically 1 fs), it is not necessary to sample the EFG at every time step. A successful strategy generally adopted in most previous works thus consists of generating a trajectory using a less expensive method than the one used to compute the EFG with a better accuracy on a limited number of configurations (or even a cluster extracted therefrom) along the trajectory. Configurations can be generated by using DFT-based ab initio MD (AIMD) followed by EFG calculations at the Hartree−Fock level,[26,27] DFT within the zeroth order relativistic approximation,[28] or an all-electron basis set instead of pseudopotentials.[29] The computational cost of AIMD typically results in poor estimates of the correlation time $\tau_c$. In addition, the small number of configurations and the fact that they are sampled from short trajectories limits the accuracy to which the ensemble average $\langle V_{zz}^2 \rangle$ can be estimated, even though the EFG is computed accurately for each configuration. The trajectory can also be obtained by classical MD and the EFG subsequently computed at the Hartree−Fock[30] or QM/MM level.[31]

Alternatively, the EFG at the site of the nucleus of interest can be determined for a given configuration using a simpler model parametrized on prior high-level calculations. On the basis of the observation of pair-additivity of the EFG on the deuterium nucleus for heavy water clusters,[32] Müller et al. proposed an analytical function to determine the EFG from the position of the neighboring atoms, parametrized on a water dimer. This model was then used to analyze classical MD trajectories of liquid water[33] and later extended to AIMD trajectories of water−DMSO mixtures.[34] Most classical MD studies rely instead on the so-called Sternheimer approximation.[35,36] The latter assumes that the electronic cloud around the nucleus responds linearly to an external EFG $V_{zz}^{ext}$, arising from the surrounding charge distribution, resulting in an additional EFG at the nucleus site. The total EFG entering in eq 1 is thus written as

$$V_{zz} = (1 + \gamma_\infty) V_{zz}^{ext} \tag{3}$$

and similarly for all Cartesian components $V_{\alpha\beta}$, with $\gamma_\infty$ being the Sternheimer antishielding factor. The contribution of the distorted electronic cloud may be much larger than the external one ($\gamma_\infty \gg 1$).[35,36]

Several caveats are in order for the use of this expression with classical MD simulations. Roberts and Schnitker underlined that "because of the uncertainty in the constants $Q$ and $\gamma_\infty$, not too much emphasis should be put on comparison of relaxation rates from experiments and simulation".[23] In addition, the validity of the Sternheimer approximation in the condensed phase has been questioned and extensions have been proposed to include higher-order terms in the electronic response.[37−39] Calandra et al. showed that short-range electronic effects, which result in reorganizations of the electronic density beyond the asymptotic (valid at large distance) linear reponse, are particularly important for anions in solids but less dramatic for cations.[40] More recently, Aidas et al. suggested that the Sternheimer approximation may not hold for aqueous $^{23}Na^{+}$, due to polarization and short-range nonelectrostatic interactions.[31] Finally, even if such an approximation applies, it should be noted that the external EFG for a given configuration depends on the charge distribution associated with the force field (FF) used to model electrostatic interactions. Therefore, the linear relation between the true $V_{zz}$ and that predicted by the classical force field $V_{zz}^{ext}$ should be verified and the corresponding effective Sternheimer antishielding factor $\gamma_{eff}$ determined accordingly.

Here we show that the EFG acf for aqueous cations can be obtained accurately in classical MD simulations using a polarizable ion model (PIM) as a FF, parametrized on ab initio calculations. The PIM, initially developed for ionic liquids and solids, describes electronic polarization via induced point dipoles and accounts for short-range electronic effects via a modification of charge−dipole interactions.[41] The force field parameters are fitted so as to best reproduce the ab initio forces and atomic dipoles from DFT calculations in the condensed phase. We have recently parametrized such a PIM for aqueous ions and validated the force field on a number of structural, thermodynamical, and dynamical properties.[42] It combines the Dang−Chang water model[43] with ion−water and ion−ion interactions of the PIM form.[44] The paper is organized as follows. In section 2, we describe the simulated system and the classical MD and DFT calculation details. We then present in section 3 the validation of the Sternheimer approximation and compare the computed NMR relaxation rates with the experimental ones.

## 2. SIMULATION DETAILS

For each of the four cations studied ($Li^{+}$, $Na^{+}$, $K^{+}$, and $Mg^{2+}$), we compute the ab initio EFG for 100 configurations from prior classical MD simulations of 1 ion and 63 water molecules in a cubic box of length 12.428 Å. Classical MD simulations over times sufficiently long (as discussed below) to correctly sample the EFG acf are performed on a larger system, consisting of ion and 215 water molecules in a cubic box of length 18.65 Å.

**2.1. Classical Simulations.** For each cation, five independent trajectories of the smaller system, of 40 ps each, are obtained after annealing at 1000 K for 200 ps followed by 200 ps equilibration at 298 K. The EFG is computed for configurations sampled every 2 ps of each trajectory, totalling 100 configurations per cation. Similarly, for the larger system, five independent trajectories of 500 ps each are obtained after annealing at 1000 K for 150 ps followed by 50 ps equilibration at 298 K and the EFG is computed every 5 fs. The cutoff radii used to compute short-range interactions are 6.2 and 9.325 Å for the smaller system and the larger system, respectively. A time step of 1 fs is used, and the temperature is maintained at $T$ = 298 K using a Nosé−Hoover thermostat[45,46] with a time constant of 1 ps.


dx.doi.org/10.1021/jp5105054 | J. Phys. Chem. B 2014, 118, 13252−13257

Classical MD simulations are performed using the polarizable ion model developed in ref 42. At each time step of the MD simulation, the dipoles are determined self-consistently by minimizing the polarization energy:

$$V_{\mathrm{pol}} = \sum_I \frac{1}{2\alpha^I} \|\mu^{\mathbf{I}}\|^2 + \sum_{I,J} [(q^I\mu_\alpha^J - q^J\mu_\alpha^I)g^{IJ}(r_{IJ})T_{IJ}^\alpha - \mu_\alpha^I\mu_\beta^J T_{IJ}^{\alpha\beta}] \quad (4)$$

with $q_I$ being the ion charge, $\alpha^I$ its isotropic polarizability, and $\mu^{\mathbf{I}}$ its induced dipole. The interaction tensors are $T_{IJ}^\alpha = \partial_\alpha(1/r_{IJ})$ and $T_{IJ}^{\alpha\beta} = \partial_\alpha\partial_\beta(1/r_{IJ})$, and the Einstein summation convention over directions $\alpha, \beta$ is assumed. A short-range correction to the multipolar expansion of the Tang–Toennies type is used:

$$g^{IJ}(r_{IJ}) = 1 - c^{IJ}e^{-b^{IJ}r_{IJ}} \sum_{k=0}^{4} \frac{(b^{IJ}r_{IJ})^k}{k!} \quad (5)$$

Once the induced dipoles are determined, including short-range electronic effects, they provide a simple description of the electronic density. In particular, we can compute the EFG generated by the set of point charges and induced dipoles (without short-range correction). Classical simulations are performed with the CP2K simulation package.[47] Electrostatic interactions and the EFG are computed using a dipolar Ewald sum,[48,49] with a tolerance of $10^{-7}$ to obtain the self-consistent dipoles.

**2.2. DFT Calculation.** In order to assess the ability of this model to capture the EFG on the ion, we compare its prediction to ab initio calculations. The projected augmented wave (PAW) method[50−53] allows the DFT-based computation of all-electron EFG in the condensed phase, i.e., using periodic boundary conditions instead of clusters. Calculations are performed with the Quantum Espresso package,[54] using the PBE functional,[55] the norm-conserving pseudopotentials provided with the QE-GIPAW Package,[56] and a kinetic energy cutoff of 80 Ry.

## 3. RESULTS AND DISCUSSION

**3.1. Validation of the Sternheimer Approximation.** Figure 1 compares the six Cartesian components of the EFG tensor computed ab initio (AI) to the prediction of the classical PIM. The results confirm the linear relation between the external EFG computed by the PIM $V_{zz}^{\mathrm{ext,PIM}}$ and the exact EFG $V_{zz}^{\mathrm{AI}}$. The slope provides the effective Sternheimer antishielding factor $\gamma_{\mathrm{eff}}$ for each ion, which can then be used to determine the classical prediction of the total EFG:

$$V_{zz}^{\mathrm{PIM}} = (1 + \gamma_{\mathrm{eff}})V_{zz}^{\mathrm{ext,PIM}} \quad (6)$$

The values are summarized in Table 1, which also reports the error on the EFG predicted by the PIM (including the Sternheimer antishielding factor) compared to the AI result, defined as

$$\sigma(V_{zz}) = \sqrt{\frac{\langle(\delta V_{zz})^2\rangle}{\langle V_{zz}{}^2\rangle}} = \sqrt{\frac{\frac{1}{N}\sum_{i=1}^{N}|V_i^{\mathrm{AI}} - V_i^{\mathrm{PIM}}|^2}{\frac{1}{N}\sum_{i=1}^{N}|V_i^{\mathrm{AI}}|^2}} \quad (7)$$

where the sums run over the six Cartesian components of the 100 configurations. As expected from the broader electronic cloud around larger ions, $\gamma_{\mathrm{eff}}$ increases from $Li^+$ to $Na^+$ and $K^+$ and slightly decreases from $Na^+$ to $Mg^{2+}$. The slope $1 + \gamma_{\mathrm{eff}}$ differs from $1 + \gamma_\infty$ (see refs 36, 38, and 39) by a factor of 1.5–1.9. Even though the EFG predicted by the PIM, eq 6, for any given configuration is not quantitative, the average error is reasonable. In addition, our sample is sufficient to determine the Sternheimer antishielding factor corresponding to the PIM with a good accuracy (uncertainties <3%) . The external EFG of the PIM combined with the effective Sternheimer antishielding factor parametrized on ab initio calculation then provides an estimate of $\langle V_{zz}{}^2\rangle$ in agreement with the AI one, as can be seen in Table 2. Even the most unfavorable case, namely, $Mg^{2+}$, is still an improvement compared to the previous calculation of ref 23.

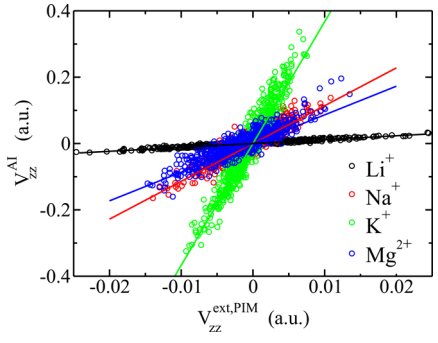


**Figure 1.** Electric field gradient: Ab initio vs polarizable ion model (PIM). For each cation, the 6 Cartesian components of the EFG tensor are reported for 100 configurations of 1 cation and 63 water molecules with periodic boundary conditions. The linear relation between the ab initio and classical results confirms the validity of the Sternheimer approximation and provides the corresponding effective antishielding factor $\gamma_{\mathrm{eff}}$ for each ion.

**Table 1. Effective Sternheimer Antishielding Factor $\gamma_{\mathrm{eff}}$ for the Polarizable Ion Model and Error $\sigma(V_{zz})$ between Its Prediction of the EFG, Taking into Account the Corresponding Effective Sternheimer Antishielding Factor, and the Ab Initio Value**

| | $\gamma_{\mathrm{eff}}$ | $\sigma(V_{zz})$ |
|---|---|---|
| $Li^+$ | 0.17 ± 0.01 | 0.29 |
| $Na^+$ | 10.4 ± 0.22 | 0.42 |
| $K^+$ | 35.7 ± 0.51 | 0.32 |
| $Mg^{2+}$ | 7.64 ± 0.21 | 0.50 |

**3.2. Comparison with Experimental Data.** Once the Sternheimer approximation is validated and the corresponding $\gamma_{\mathrm{eff}}$ determined, we can perform classical MD simulations of a larger system over times sufficiently long to correctly sample the EFG acf. The simulated system contains one ion and 215 water molecules in a cubic box of length 18.65 Å. A time step of

**Table 2. Variance of the EFG $\langle V_{zz}{}^2\rangle$ (in Atomic Units) Obtained from Ab Initio (AI) Calculations and with the Polarizable Ion Model (PIM)**

| | $\langle V_{zz}{}^2\rangle$ (a.u.) | |
|---|---|---|
| | AI | PIM |
| $Li^+$ | $(8.94 \pm 2.47) \times 10^{-5}$ | $(8.18 \pm 2.19) \times 10^{-5}$ |
| $Na^+$ | $(2.37 \pm 0.34) \times 10^{-3}$ | $(1.95 \pm 0.26) \times 10^{-3}$ |
| $K^+$ | $(1.32 \pm 0.14) \times 10^{-2}$ | $(1.19 \pm 0.14) \times 10^{-2}$ |
| $Mg^{2+}$ | $(2.25 \pm 0.41) \times 10^{-3}$ | $(1.68 \pm 0.23) \times 10^{-3}$ |


dx.doi.org/10.1021/jp5105054 | J. Phys. Chem. B 2014, 118, 13252−13257

Table 3. Variance of the External and Total EFG (Atomic Units) and EFG Correlation Time $\tau_c$ from 5 × 500 ps Simulations of the Large System Using the PIM[a]

| | $\langle(V_{zz}^{ext})^2\rangle$ (a.u.) | $\langle V_{zz}^2\rangle$ (a.u.) | $\tau_c$ (fs) | $1/T_1^{PIM}$ ($s^{-1}$) | $1/T_1^{exp}$ ($s^{-1}$) |
|---|---|---|---|---|---|
| $^7Li^+$ | (7.44 ± 0.16) × $10^{-5}$ | (1.02 ± 0.02) × $10^{-4}$ | 180 | 3.22 × $10^{-2}$ | 2.70 × $10^{-2}$ |
| $^{23}Na^+$ | (1.56 ± 0.02) × $10^{-5}$ | (2.03 ± 0.03) × $10^{-3}$ | 285 | 7.07 | 16.2 |
| $^{39}K^+$ | (8.36 ± 0.09) × $10^{-6}$ | (1.13 ± 0.01) × $10^{-2}$ | 375 | 16.1 | 17.8 |
| $^{25}Mg^{2+}$ | (2.45 ± 0.06) × $10^{-5}$ | (1.83 ± 0.04) × $10^{-3}$ | 110 | 3.04 | 4.16 |

[a]The corresponding relaxation rate $1/T_1$ is compared to the experimental result.[4,6,57]

1 fs is used, and the temperature is maintained at $T$ = 298 K using a Nosé−Hoover thermostat[45,46] with a time constant of 1 ps. For each cation, the EFG acf is computed from five independent trajectories of 500 ps each. The EFG variances $\langle(V_{zz}^{ext})^2\rangle$ and $\langle V_{zz}^2\rangle$ are given in Table 3. Results for the latter are consistent with the one obtained for the smaller systems with a more limited number of configurations (see Table 2). This is due to the fact that the EFG on the ion depends mainly on the first solvation shell. The $\langle V_{zz}^2\rangle$ for $Li^+$ and $Na^+$ are consistent with previous ab initio calculations.[19,20,22,28] To the best of our knowledge, no such ab initio data is available for $K^+$ and $Mg^{2+}$.

Increasing the ion radius from $Li^+$ to $Na^+$ and from $Na^+$ to $K^+$ results in an increase in $\langle V_{zz}^2\rangle$ by a factor of 20 and 10, respectively. Increasing the charge from $Na^+$ to $Mg^{2+}$, it decreases slightly (as does the ionic radius). These variations are essentially due to the variations of the antishielding factor $\gamma_\infty$. Indeed, the fluctuations of the external EFG $\langle(V_{zz}^{ext})^2\rangle$ follow the opposite trends (see Table 3), in qualitative agreement with the results obtained by Roberts and Schnitker with a simpler force field.[23] Two effects result in a smaller EFG: First, with larger ions, each water molecule that is further from the nucleus contributes less to the EFG; second, the larger number of such molecules results in compensations between them.

The EFG acf are finally reported in Figure 2. Results indicate averages over the five trajectories, together with the corresponding standard deviations. The moderate computational cost of classical MD with the PIM, compared to AIMD, therefore allows a sufficient sampling of the acf to obtain the correlation time $\tau_c$ with a good accuracy (Figure 3). Note that the results are normalized by the initial value of the acf to facilitate the comparison between ions. The decay is not monoexponential, and the acf displays a fast initial decrease over ∼100 fs followed by a slower decorrelation over a few ps, in agreement with previous findings.[22,23] In the case of $Li^+$, the acf oscillates with a period of ∼85 fs. Such oscillations of the EFG acf have not been reported in previous works[23,25] but are consistent (with the same period) with those observed for that of the velocity (VACF) and force (FACF)[58] and correspond to the rattling of the light $Li^+$ inside its solvation shell. For $Mg^{2+}$, one also observes an oscillation, with a negative part. The correlation time $\tau_c$ (Table 3) increases from $Li^+$ to $Na^+$ and decreases from $Na^+$ to $Mg^{2+}$. The microscopic mechanisms leading to the observed behaviors will be discussed elsewhere.

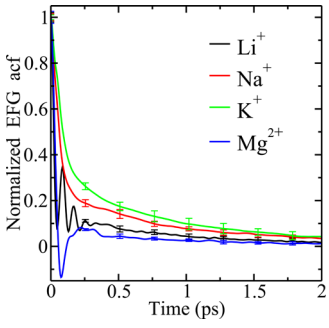


Figure 2. Electric field gradient autocorrelation function, normalized by their initial value $\langle V_{zz}^2\rangle$, for $Li^+$, $Na^+$, $K^+$, and $Mg^{2+}$.

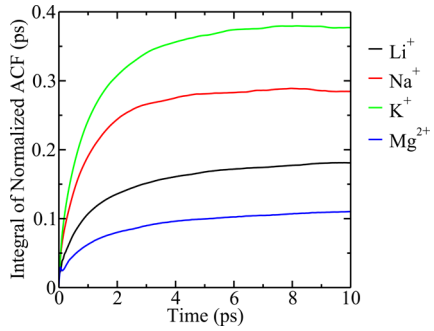


Figure 3. Integral of the normalized electric field gradient autocorrelation function, normalized by their initial value $\langle V_{zz}^2\rangle$. The plateau gives the correlation time $\tau_c$.

The time integrals, used to compute the correlation time $\tau_c$, are illustrated in Figure 3, which clearly shows that the EFG acf must be computed accurately over several picoseconds in order to reach the plateau corresponding to $\tau_c$. This underlines the difficulty to determine the latter from AIMD only. Finally, Table 3 also compares the relaxation rates $1/T_1$ obtained by eq 1, using $\langle V_{zz}^2\rangle$ and $\tau_c$ computed with the PIM and quadrupole moments from ref 59. The results agree very well with the experimental values,[4,57] to within a factor of 2.3 in the worse case ($Na^+$) and only 10% for $K^+$. The agreement for $Mg^{2+}$ (within 25%) is remarkable, as the only previous estimate from MD simulations would differ by a factor of 20.[23] This confirms the ability of the PIM force field of ref 42 to describe this multivalent ion and its solvation shell. Note that for $^7Li^+$ dipole−dipole relaxation may contribute to the measured relaxation rate: The larger MD value should therefore be an overestimate of the quadrupolar contribution considered here. The relative weight of the dipole−dipole mechanism could be investigated in a future work.[25]

## 4. CONCLUSION

In conclusion, combining classical MD with an accurate force field parametrized on ab initio simulation with the prior determination of Sternheimer antishielding factors by comparing the classical and ab initio EFG provides an efficient route to NMR quadrupolar relaxation rates. This allows computing both $\langle V_{zz}^2\rangle$ and $\tau_c$, in contrast with more computationally demanding approaches based on AIMD, whose cost prevents the required sampling of trajectories. The advantage of the present strategy would be even more evident for systems where


dx.doi.org/10.1021/jp5105054 | J. Phys. Chem. B 2014, 118, 13252−13257

the EFG evolves over longer time scales than the present case of aqueous ions at infinite dilution. We are currently applying it to the case of silicate glasses where a full AIMD determination is currently out of reach. Note that the contribution of dipole−dipole relaxation can also be determined from the classical trajectories.[24,25]

Just as the accuracy of the PIM force field, the determination of the Sternheimer antishielding factor is limited by the quality of the AI calculations. More importantly, comparing the classical and AI EFG on the same configurations allows the validity of the Sternheimer approximation to be assessed. In cases where it cannot be applied (it is expected to be less satisfactory for anions, for example[40]), it would be possible to analyze the configurations of the classical MD including higher order terms,[37−39] or even to parametrize a hypersurface based on the local configuration around the nucleus.[33,34] The accurate computation of the EFG acf on the molecular scale, or in the case of the anisotropic environment of the nuclear quadrupole coupling constant, could then be coupled to coarse-grained simulations in the framework of a multiscale approach for complex materials.[60]

## AUTHOR INFORMATION


### Corresponding Author

*E-mail: benjamin.rotenberg@upmc.fr.


### Notes

The authors declare no competing financial interest.

## ACKNOWLEDGMENTS

The authors thank Paul Madden and Guillaume Mériguet for insightful discussions. A.C. acknowledges financial support from UPMC. T.C. thanks the CCRT and the Grand Equipement National de Calcul Intensif (grant 096303) for access to HPC resources.

## REFERENCES


(1) Abragam, A. *Principles of Nuclear Magnetism*, 2nd ed.; Oxford University Press: Oxford, 1983.

(2) Laage, D.; Hynes, J. T. A Molecular Jump Mechanism of Water Reorientation. *Science* **2006**, *311*, 832−835.

(3) Kowalewski, J.; Maler, L. *Nuclear Spin Relaxation in Liquids: Theory, Experiments, and Applications*; CRC Press: New York, 2006.

(4) Hertz, H. G. Magnetic-Relaxation by Quadrupole Interaction of Ionic Nuclei in Electrolyte Solutions 1. Limiting Values for Infinite Dilution. *Ber. Bunsen-Ges.* **1973**, *77*, 531−540.

(5) Hertz, H. G. Magnetic-Relaxation by Quadrupole Interaction of Ionic Nuclei in Electrolyte Solutions 2. Relaxation at Finite Ion Concentrations. *Ber. Bunsen-Ges.* **1973**, *77*, 688−697.

(6) Weingärtner, H.; Hertz, H. G. Magnetic Relaxation by Quadrupolar Interaction of Ionic Nuclei in Non-Aqueous Electrolyte Solutions. Part I. Limiting Values for Infinite Dilution. *Ber. Bunsen-Ges.* **1977**, *81*, 1204−1221.

(7) Sacco, A. Structure and Dynamics of Electrolyte Solutions. A NMR Relaxation Approach. *Chem. Soc. Rev.* **1994**, *23*, 129−136.

(8) Engelhardt, G.; Michel, D. *High-Resolution Solid-State NMR of Silicates and Zeolites*; John Wiley & Sons: Chichester, U.K., 1987.

(9) Grey, C. P.; Poshni, F. I.; Gualtieri, A. F.; Norby, P.; Hanson, J. C.; Corbin, D. R. Combined MAS NMR and X-ray Powder Diffraction Structural Characterization of Hydrofluorocarbon-134 Adsorbed on Zeolite NaY: Observation of Cation Migration and Strong Sorbate-Cation Interactions. *J. Am. Chem. Soc.* **1997**, *119*, 1981−1989.

(10) Porion, P.; Faugère, A. M.; Delville, A. $^{1}$H and $^{7}$Li NMR Pulsed Gradient Spin Echo Measurements and Multiscale Modeling of the Water and Ionic Mobility within Aqueous Dispersions of Charged Anisotropic Nanoparticles. *J. Phys. Chem. C* **2008**, *112*, 11893−11900.

(11) Porion, P.; Faugère, A. M.; Delville, A. $^{7}$Li NMR Spectroscopy and Multiquantum Relaxation as a Probe of the Microstructure and Dynamics of Confined $Li^+$ Cations: An Application to Dense Clay Sediments. *J. Phys. Chem. C* **2008**, *112*, 9808−9821.

(12) Porion, P.; Delville, A. Multinuclear NMR Study of the Structure and Micro-Dynamics of Counterions and Water Molecules within Clay Colloids. *Curr. Opin. Colloid Interface Sci.* **2009**, *14*, 216−222.

(13) Edén, M. NMR Studies of Oxide-Based Glasses. *Annu. Rep. Prog. Chem., Sect. C: Phys. Chem.* **2012**, *108*, 177.

(14) Charpentier, T.; Menziani, M. C.; Pedone, A. Computational Simulations of Solid State NMR Spectra: a New Era in Structure Determination of Oxide Glasses. *R. Soc. Chem. Adv.* **2013**, *3*, 10550.

(15) Nordenskiold, L.; Chang, D. K.; Anderson, C. F.; Record, M. T. Sodium-23 NMR Relaxation Study of the Effects of Conformation and Base Composition on the Interactions of Counterions with Double-Helical DNA. *Biochemistry* **1984**, *23*, 4309−4317.

(16) Wolynes, P. G. Dynamics of Electrolyte Solutions. *Annu. Rev. Phys. Chem.* **1980**, *31*, 345−376.

(17) Chen, J.-H.; Adelman, S. A. Macroscopic Model for Solvated Ion Dynamics. *J. Chem. Phys.* **1980**, *72*, 2819−2831.

(18) Hynes, J. T.; Wolynes, P. G. A Continuum Theory for Quadrupole Relaxation of Ions in Solution. *J. Chem. Phys.* **1981**, *75*, 395−401.

(19) Engström, S.; Jönsson, B. Monte Carlo Simulations of the Electric Field Gradient Fluctuation at the Nucleus of a Lithium Ion in Dilute Aqueous Solution. *Mol. Phys.* **1981**, *43*, 1235−1253.

(20) Engström, S.; Jönsson, B.; Jönsson, B. A Molecular Approach to Quadrupole Relaxation. Monte Carlo Simulations of Dilute $Li^+$, $Na^+$, and $Cl^-$ Aqueous Solutions. *J. Magn. Reson. (1969-1992)* **1982**, *50*, 1−20.

(21) Linse, P.; Halle, B. Counterion NMR in Heterogeneous Aqueous Systems: A Molecular Dynamics Simulation Study of the Electric Field Gradient. *Mol. Phys.* **1989**, *67*, 537−573.

(22) Engström, S.; Jönsson, B.; Impey, R. W. Molecular Dynamic Simulation of Quadrupole Relaxation of Atomic Ions in Aqueous Solution. *J. Chem. Phys.* **1984**, *80*, 5481−5486.

(23) Roberts, J. E.; Schnitker, J. Ionic Quadrupolar Relaxation in Aqueous Solution: Dynamics of the Hydration Sphere. *J. Phys. Chem.* **1993**, *97*, 5410−5417.

(24) Odelius, M.; Laaksonen, A.; Levitt, M. H.; Kowalewski, J. Intermolecular Dipole-Dipole Relaxation. A Molecular Dynamics Simulation. *J. Magn. Reson., Ser. A* **1993**, *105*, 289−294.

(25) Odelius, M.; Kowalewski, J. Molecular Dynamics Simulation of Nuclear Spin Relaxation of $^{7}Li^+$ in Water. *J. Chem. Soc., Faraday Trans.* **1995**, *91*, 215−222.

(26) Kirchner, B.; Searles, D. J.; Dyson, A. J.; Vogt, P. S.; Huber, H. Disproving the Iceberg Effect? A Study of the Deuteron Quadrupole Coupling Constant of Water in a Mixture with Dimethyl Sulfoxide via Computer Simulations. *J. Am. Chem. Soc.* **2000**, *122*, 5379−5383.

(27) Pennanen, T. S.; Vaara, J.; Lantto, P.; Sillanpää, A. J.; Laasonen, K.; Jokisaari, J. Nuclear Magnetic Resonance Chemical Shifts and Quadrupole Couplings for Different Hydrogen-Bonding Cases Occurring in Liquid Water: A Computational Study. *J. Am. Chem. Soc.* **2004**, *126*, 11093−11102.

(28) Badu, S.; Truflandier, L.; Autschbach, J. Quadrupolar NMR Spin Relaxation Calculated Using Ab Initio Molecular Dynamics: Group 1 and Group 17 Ions in Aqueous Solution. *J. Chem. Theory Comput.* **2013**, *9*, 4074−4086.

(29) Schmidt, J.; Hutter, J.; Spiess, H.-W.; Sebastiani, D. Beyond Isotropic Tumbling Models: Nuclear Spin Relaxation in Liquids from First Principles. *ChemPhysChem* **2008**, *9*, 2313−2316.

(30) Baumert, R.; Ludwig, R.; Geiger, A. Quadrupole Relaxation of the $^{7}Li^+$ Ion in Dilute Aqueous Solution Determined by Experimental and Theoretical Methods. *J. Mol. Model.* **1996**, *2*, 379−382.

(31) Aidas, K.; Ågren, H.; Kongsted, J.; Laaksonen, A.; Mocci, F. A Quantum Mechanics/Molecular Dynamics Study of Electric Field Gradient Fluctuations in the Liquid Phase. The Case of $Na^+$ in Aqueous Solution. *Phys. Chem. Chem. Phys.* **2013**, *15*, 1621−1631.

(32) Müller, M. G.; Kirchner, B.; Vogt, P. S.; Huber, H.; Searles, D. J. Electric Field Gradients are Highly Pair-Additive. *Chem. Phys. Lett.* **2001**, *346*, 160−162.
(33) Hardy, E. H.; Müller, M. G.; Vogt, P. S.; Bratschi, C.; Kirchner, B.; Huber, H.; Searles, D. J. How Approximate is the Experimental Evaluation of Quadrupole Coupling Constants in Liquids? A Novel Computational Study. *J. Chem. Phys.* **2003**, *119*, 6184−6193.
(34) Müller, M. G.; Hardy, E. H.; Vogt, P. S.; Bratschi, C.; Kirchner, B.; Huber, H.; Searles, D. J. Calculation of the Deuteron Quadrupole Relaxation Rate in a Mixture of Water and Dimethyl Sulfoxide. *J. Am. Chem. Soc.* **2004**, *126*, 4704−4710.
(35) Sternheimer, R. M. Shielding and Antishielding Effects for Various Ions and Atomic Systems. *Phys. Rev.* **1966**, *146*, 140−160.
(36) Schmidt, P. C.; Sen, K. D.; Das, T. P.; Weiss, A. Effect of Self-Consistency and Crystalline Potential in the Solid State on Nuclear Quadrupole Sternheimer Antishielding Factors in Closed-Shell Ions. *Phys. Rev. B* **1980**, *22*, 4167−4179.
(37) Buckingham, A. D. Nuclear Quadrupole Coupling in Ionic Molecules. *Trans. Faraday Soc.* **1962**, *58*, 1277.
(38) Fowler, P. W. Hyperpolarisation Effects on the Electric Field Gradient at a Nucleus. *Chem. Phys. Lett.* **1989**, *156*, 494−500.
(39) Bacskay, G. B.; Buckingham, A. D. Nuclear Quadrupole Coupling Constants in Alkali Halide Molecules: an *Ab Initio* Quantum Chemical Study. *Mol. Phys.* **1997**, *91*, 391−400.
(40) Calandra, P.; Domene, C.; Fowler, P. W.; Madden, P. A. Nuclear Quadrupole Coupling of $^{17}$O and $^{33}$S in Ionic Solids: Invalidation of the Sternheimer Model by Short-Range Corrections. *J. Phys. Chem. B* **2002**, *106*, 10342−10348.
(41) Salanne, M.; Rotenberg, B.; Jahn, S.; Vuilleumier, R.; Simon, C.; Madden, P. A. Including Many-Body Effects in Models for Ionic Liquids. *Theor. Chem. Acc.* **2012**, *131*, 1−16.
(42) Tazi, S.; Molina, J. J.; Rotenberg, B.; Turq, P.; Vuilleumier, R.; Salanne, M. A Transferable Ab Initio Based Force Field for Aqueous Ions. *J. Chem. Phys.* **2012**, *136*, 114507.
(43) Dang, L. X.; Chang, T.-M. Molecular Dynamics Study of Water Clusters, Liquid, and Liquid-Vapor Interface of Water with Many-Body Potentials. *J. Chem. Phys.* **1997**, *106*, 8149−8159.
(44) In ref 24, the polarizability of the cations was found to be negligible and therefore set to zero. Nevertheless, we refer to the force field as the polarizable ion model.
(45) Nosé, S. A Molecular Dynamics Method for Simulations in the Canonical Ensemble. *Mol. Phys.* **1984**, *52*, 255−268.
(46) Nosé, S. A unified formulation of the constant temperature molecular dynamics methods. *J. Chem. Phys.* **1984**, *81*, 511.
(47) CP2K developers group; www.cp2k.org.
(48) Aguado, A.; Madden, P. A. Ewald Summation of Electrostatic Multipole Interactions up to the Quadrupolar Level. *J. Chem. Phys.* **2003**, *119*, 7471.
(49) Laino, T.; Hutter, J. Notes on "Ewald Summation of Electrostatic Multipole Interactions up to Quadrupolar Level" [J. Chem. Phys. 119, 7471 (2003)]. *J. Chem. Phys.* **2008**, *129*, 074102.
(50) Van de Walle, C. G.; Blöchl, P. E. First-Principles Calculations of Hyperfine Parameters. *Phys. Rev. B 47*, 4244−4255.
(51) Blöchl, P. E. Projector Augmented-Wave Method. *Phys. Rev. B 50*, 17953−17979.
(52) Charpentier, T. The PAW/GIPAW Approach for Computing NMR Parameters: A New Dimension Added to NMR Study of Solids. *Solid State Nucl. Magn. Reson.* **2011**, *40*, 1−20.
(53) Bonhomme, C.; Gervais, C.; Babonneau, F.; Coelho, C.; Pourpoint, F.; Azaïs, T.; Ashbrook, S. E.; Griffin, J. M.; Yates, J. R.; Mauri, F.; et al. First-Principles Calculation of NMR Parameters Using the Gauge Including Projector Augmented Wave Method: A Chemist's Point of View. *Chem. Rev.* **2012**, *112*, 5733−5779.
(54) Giannozzi, P.; Baroni, S.; Bonini, N.; Calandra, M.; Car, R.; Cavazzoni, C.; Ceresoli, D.; Chiarotti, G. L.; Cococcioni, M.; Dabo, I.; et al. QUANTUM ESPRESSO: a Modular and Open-Source Software Project for Quantum Simulations of Materials. *J. Phys.: Condens. Matter* **2009**, *21*, 395502.
(55) Perdew, J. P.; Burke, K.; Ernzerhof, M. Generalized Gradient Approximation Made Simple. *Phys. Rev. Lett.* **1996**, *77*, 3865−3868.
(56) GIPAW norm-conserving pseudopotentials; https://sites.google.com/site/dceresoli/pseudopotentials.
(57) Struis, R. P. W. J.; De Bleijser, J.; Leyte, J. C. Magnesium-25(2+) and Chloride-35 Quadrupolar Relaxation in Aqueous Magnesium Chloride Solutions at 25°C. 1. Limiting Behavior for Infinite Dilution. *J. Phys. Chem.* **1989**, *93*, 7932−7942.
(58) Koneshan, S.; Rasaiah, J. C.; Lynden-Bell, R. M.; Lee, S. H. Solvent Structure, Dynamics, and Ion Mobility in Aqueous Solutions at 25°C. *J. Phys. Chem. B* **1998**, *102*, 4193−4204.
(59) Pyykkö, P. Year-2008 Nuclear Quadrupole Moments. *Mol. Phys.* **2008**, *106*, 1965−1974.
(60) Porion, P.; Faugère, A. M.; Delville, A. Multinuclear NMR Study of the Structure and Micro-Dynamics of Counterions and Water Molecules within Clay Colloids. *J. Phys. Chem. C* **2013**, *117*, 26119−26134.